Journal of Applied Polymer Science

Autonomic self-healing of poly(vinyl butyral)

Sunatda Arayachukiat,[1] Vu Anh Doan,[1,2] Tatsuya Murakami,[3] Shogo Nobukawa,[1] Masayuki Yamaguchi[1]

[1]School of Materials Science, Japan Advanced Institute of Science and Technology, Nomi, Ishikawa 923-1292, Japan
[2]Department of Textile Materials and Chemistry Technology, School of Textile-Leather and Fashion, Hanoi University of Science and Technology, Hai Ba Trung, Ha Noi, Vietnam
[3]Center for Nano Materials and Technology, Japan Advanced Institute of Science and Technology, Ishikawa 923-1292, Japan
Correspondence to: M. Yamaguchi (E-mail: m_yama@jaist.ac.jp)

ABSTRACT: The self-healing behavior of poly(vinyl butyral) (PVB) is evaluated below the glass transition temperature T_g. It is found that PVB shows autonomic self-healing even at room temperature, although T_g is around at 76°C. Furthermore, a large amount of water is found to be adsorbed on the surface of the film. This is attributed to the surface localization of hydroxyl group in PVB, which is confirmed by X-ray photoelectron spectroscopy. Since the surface is plasticized by water, the scar applied by a razor blade is healed even in the glassy state of the bulk. Moreover, the healing efficiency is enhanced at high humidity condition, owing to the pronounced plasticizing effect by water. © 2015 Wiley Periodicals, Inc. J. Appl. Polym. Sci. **2015**, *132*, 42008.

KEYWORDS: rheology; stimuli-sensitive polymers; structure–property relations; surfaces and interfaces; thermoplastics

Received 10 November 2014; accepted 19 January 2015
DOI: 10.1002/app.42008

INTRODUCTION

Self-healing is one of the desirable biomimetic properties in which materials have the ability to restore their original properties when they are damaged. This is an attractive and valuable nature, since it can effectively lead to the lengthening of the lifespan of a product made from such materials. Up to now, various methods, summarized in the literature,[1–6] have been proposed to provide this function to polymeric materials as one of the biomimetic properties. Because self-healing phenomenon can be regarded as the adhesion between the cut surfaces, various adhesive mechanisms have been utilized for the material design. These include; chemical reaction, intermolecular interaction between specific functions, anchor effect and chain interdiffusion. Among these mechanisms, chemical reaction has been the most widely studied.

Composites with microcapsules[7–11] and hollow fibers,[12–14] in which a healing agent is loaded, have been developed after the pioneering works by White *et al.*[7] and Dry.[12] Reversible chemical reactions such as Diels-Alder/Retro Diels-Alder have been focused to develop thermally reversible gels.[15,16] Another famous reversible reaction, that is available to develop a self-healing polymer, is photo-induced cycloaddition of coumarin.[17]

Intermolecular interactions between specific groups are also employed, such as hydrogen bonding,[18–22] ionic interaction in ionomers,[23,24] and π–π stacking interaction.[25] Furthermore, the addition of thermoplastics into a thermoset resin was proposed,[26–28] which is based on a similar concept to that of the anchor effect at adhesion.

Moreover, the chain interdiffusion, which is also used for an adhesion method available only for a polymer, has been known to show the recovery of mechanically induced damages beyond the glass transition temperature T_g, which is called "crack healing."[29] Although the technique needs the manual operation to rise the ambient temperature for the repair, Yamaguchi *et al.* demonstrated that a weak gel with low T_g exhibits autonomic healing owing to the interdiffusion of dangling chains.[30–32] The mechanism of crack healing has been summarized and explained by Wool using the minor chain model[29] based on the reptation concept.[33] Furthermore, Brown *et al.* studied the relation between the interdiffusion of aromatic polyimide and the adhesive strength.[34] They found that at least 200 nm is required as the diffusion distance in order to exhibit good mechanical strength. Their results suggest that chain mobility at surface is important for the healing. In the meantime, Kajiyama *et al.* revealed that T_g at surface is lower than that of the bulk.[35] According to them, the marked molecular motion at the surface was explained in term of the chain end effect and reduced chain cooperativity by the large free volume on surface. Moreover, the surface region also possesses specific chain conformation, which is different from the bulk region.[35–37]

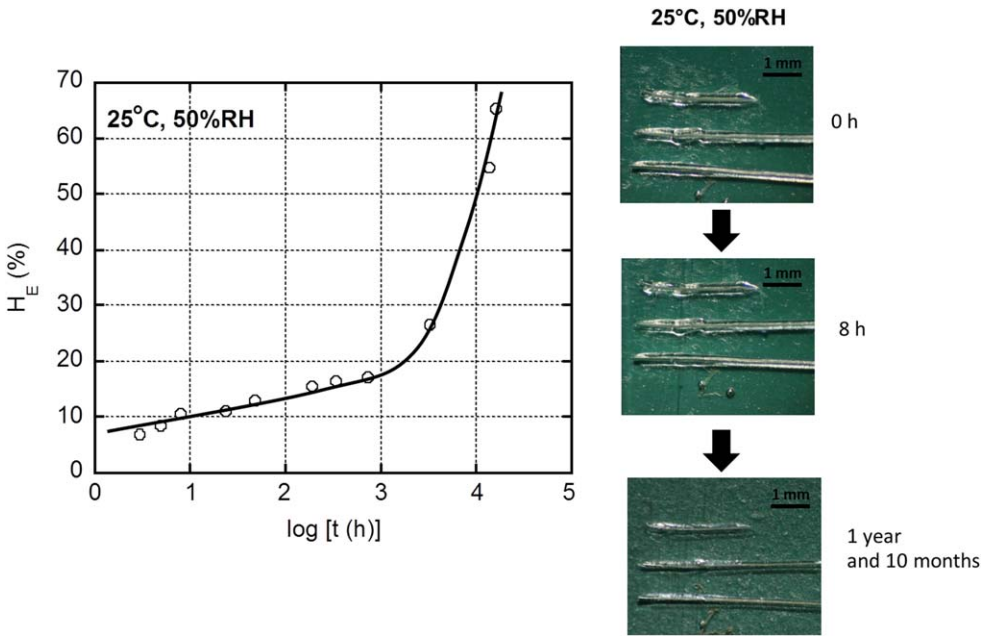

Figure 1. Self-healing behavior at 25°C and 50% RH; (left) healing efficiency as a function of time and (right) the sample surface at (top) $t = 0$, (middle) $t = 8$ h, and (bottom) $t = 16{,}104$ h (1 year and 10 months). [Color figure can be viewed in the online issue, which is available at wileyonlinelibrary.com].

In this work, an amorphous terpolymer composed of vinyl butyral, vinyl alcohol, and vinyl acetate is employed to demonstrate the healing behavior by molecular motion at surface even below T_g. Since neither manual operation nor chemical reaction is required for healing, the industrial application will be considered.

EXPERIMENTAL

Material

A polymer used in this study was a commercially available terpolymer composed of vinyl butyral (79 wt %, 55 mol %), vinyl alcohol (19 wt %, 42.7 mol %), and vinyl acetate (2 wt %, 2.3 mol %) (Denki Kagaku Kogyo, Japan, Denka PVB 4000-2). In this study, the sample is denoted as poly(vinyl butyral) (PVB). The number- and weight-average molecular weights, evaluated by a size exclusion chromatography (Tosoh, Japan, HLC-8020) using chloroform as a solvent, were $M_n = 1.1 \times 10^5$ and $M_w = 2.2 \times 10^5$ as a polystyrene standard. Furthermore, the sample has no crystalline phase with T_g of 76°C, which were evaluated by DSC measurements at 10°C/min. Other basic characterizations were performed in our previous article.[38]

After being dried, PVB was compressed into flat sheets with various thicknesses by a compression-molding machine (Tester Sangyo, Japan, Table-type test-press) at 190°C under 10 MPa for 3 min. Then, the samples were rapidly cooled down in an ice-water bath.

Measurements

The healing behavior was evaluated using the sample films with 300 μm of the thickness. The surface of the film was cut by a razor blade. The initial depth of the scar was approximately 35 μm. Then, the sample was annealed at 25°C under 50% of relative humidity (50% RH) for various periods up to 1 year and 8 months. The effect of humidity on the healing was studied by exposure to annealing operation with two levels of RH, i.e., 10% RH and 95% RH, for 8 h. The annealing temperature was controlled at T_g—20°C (56°C). The sample surface was observed by a stereomicroscope before and after the annealing procedure. Furthermore, the depths of the scar were evaluated by a roughness tester (Time, Japan, TR200) to calculate the healing efficiency H_E defined as follows;

$$H_E\ (\%) = \frac{D_i - D(t)}{D_i} \times 100 \qquad (1)$$

where D_i is the initial depth of the scar and $D(t)$ is that after t hours.

The film surface was characterized by attenuated total reflectance Fourier-transform infrared spectroscopy (ATR-FTIR) (Perkin Elmer, UK, Spectrum 100 FT-IR spectrometer) at room temperature. The KRS-5 and Germanium were used as ATR crystals. Prior to the measurements, the sample was kept in an incubator at 25°C under vacuum for 1 day.

The surface functional groups were characterized by X-ray photoelectron spectroscopy (XPS) (Kratos, UK, Kratos AXIS Ultra DLD instrument) using a monochromatic Al Kα X-ray source at 1486.6 eV and operated at 15 kV and 10 mA with a base pressure in the XPS analysis chamber of 6.67×10^{-6} Pa. High resolution spectrum (C1s) was acquired using a pass energy of 20 eV and 0.1 eV energy steps. All binding energies (BEs) were referenced to the hydrocarbon C1s peak at 284.5 eV. The samples were kept under vacuum at 25°C for 2 days before the measurement.

The water content was evaluated using a moisturemeter (Mitsubishi Chemical Corporation, Japan, CA-200) using the Karl Fischer method, in which the Karl Fischer reagent, which

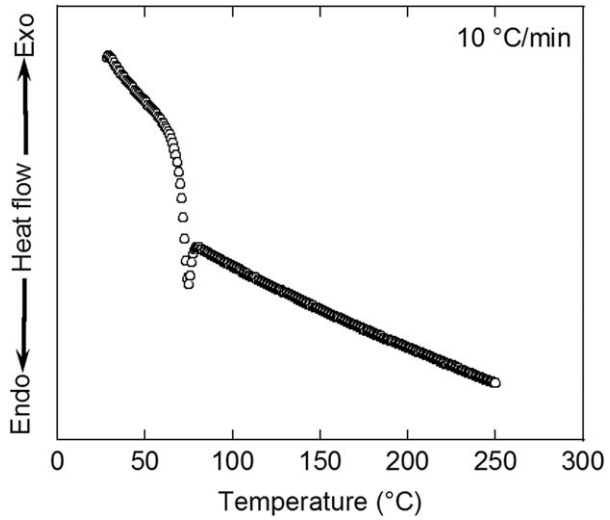

Figure 2. DSC heating curve at a heating rate of 10°C/min.

consists of iodine, sulfur dioxide, a base and a solvent, reacts quantitatively and selectively with water. The square (10 mm × 10 mm) films with various thicknesses were used to evaluate the effect of the film thickness on the water content, which provides the information on the water content on the surface as well as in the bulk. The films were kept in a humidic chamber at 25°C under 50% RH for 8 h before the measurement. The measurements were conducted at 180°C under a nitrogen atmosphere at a flow rate of 250 mL/min.

Temperature dependence of oscillatory tensile moduli such as storage modulus E' and loss modulus E'' was measured from −10 to 120°C by a dynamic mechanical analyzer (UBM, Japan, E-4000) using rectangular specimens with 5 mm in width, 20 mm in length, and 300 μm in thickness. The frequency was 10 Hz and the heating rate was 2°C/min. Prior to the measurements, the samples were kept at 25°C for 8 h under either vacuum or 50% RH.

Thermal properties were evaluated by a differential scanning calorimeter (Mettler Toledo, UK, DSC820) under a nitrogen atmosphere. The samples were heated from room temperature to 250°C at a heating rate of 10°C/min. The amount of the sample in an aluminum pan was approximately 10 mg.

RESULTS AND DISCUSSION

The healing behavior at 25°C under 50% RH is exemplified in Figure 1. Apparently, the scar applied by a razor blade is healed to some extent even at room temperature, although the storage modulus at room temperature is around 1 GPa, i.e., glassy state. As well known, PVB has no crystalline part, which was confirmed by DSC in Figure 2. The figure demonstrates that PVB used in this study is a typical amorphous polymer with T_g of 75°C.

As seen in Figure 1, the healing efficiency increases with time. The result indicates that the molecular motion is not fully inhibited even below T_g. The good healing behavior can be attributed to the pronounced molecular motion at surface due to the excess free volume. In fact, Tanaka *et al.* demonstrated

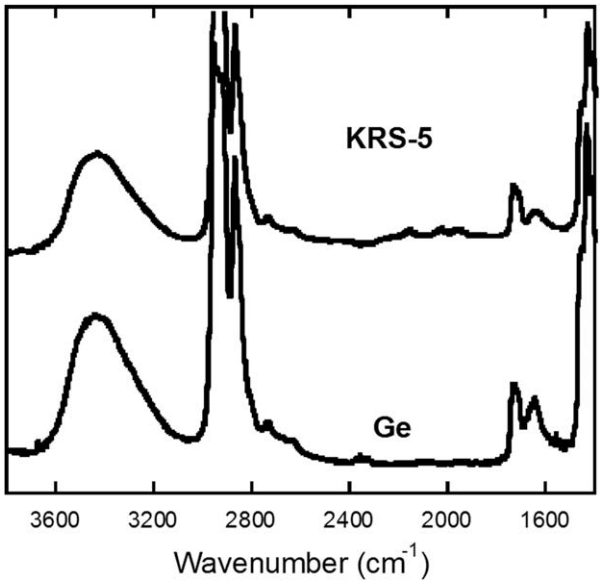

Figure 3. ATR-FTIR spectra measured using (top) KRS-5 and (bottom) Germanium as ATR plates.

that T_g at surface is lower than T_g of the bulk by lateral force microscopy.[36,37] However, even considering the marked molecular motion at surface, the healing behavior of PVB should be noted, because other plastics with similar T_g, e.g., poly(lactic acid) and poly(ethylene terephthalate), do not show such a good healing behavior at room temperature. Therefore, another mechanism should be taken into consideration.

To investigate the functional groups at the surface, ATR-FTIR analysis with different ATR crystals such as Germanium and KRS-5 was performed. The penetration depth of the IR beam d_p is provided by the following equation,

$$d_p = \frac{\lambda}{2\pi\sqrt{\sin^2\theta - (n_2 - n_1)^2}} \quad (2)$$

where n_1 is the refractive index of the crystal, n_2 is that of the sample, λ is the wavelength of light and θ is the angle of incidence of the IR beam relative to a perpendicular from the surface of the crystal. Because the refractive indices of Germanium and KRS-5 are 4.0 and 2.4, respectively, the information on the different penetration depth is obtained using the plates.

As shown in Figure 3, the ATR-FTIR spectra show O—H stretching at 3000–3600 cm^{-1} and C═O stretching at 1600–1800 cm^{-1}. The CO peak originates from vinyl acetate in PVB, whereas the OH peak is from either vinyl alcohol and/or the moisture adsorbed on the surface. According to eq. (2), the penetration depth of the IR beam into the sample at 3430 cm^{-1} is approximately 190 nm and 565 nm for Germanium and KRS-5 crystals, respectively. Further, the absorption ratios of OH/CO are 105 and 14 for Germanium and KRS-5 crystals, respectively. This indicates that the surface has more hydroxyl group and/or the moisture.

Figure 4 shows the XPS spectrum of the sample dried under vacuum for 2 days prior to the measurement. Since the

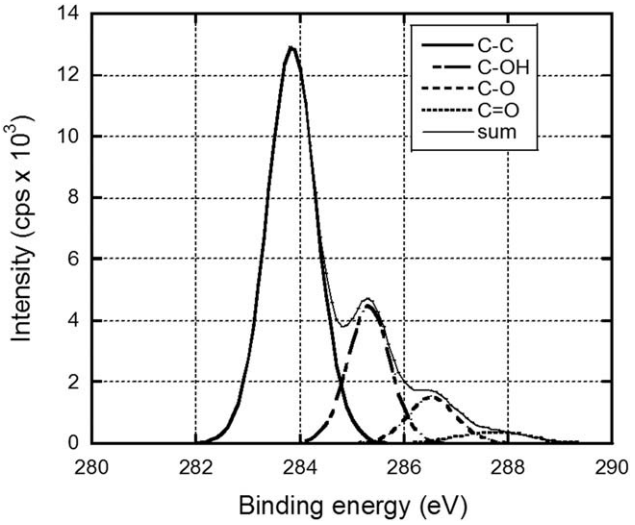

Figure 4. XPS spectra of the film.

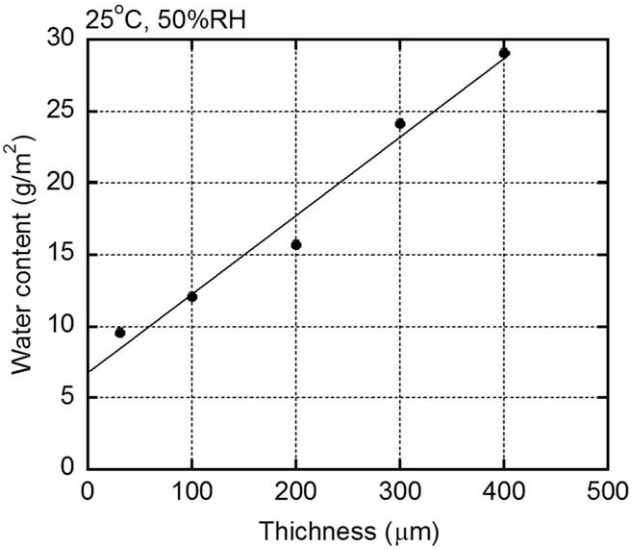

Figure 5. Water content per unit area of the sample films with various thicknesses. The samples were kept at 25°C and 50% RH for 8 h.

measurement was performed under vacuum condition, the effect of the moisture is minimized. The XPS spectrum reveals that the functional groups at the surface are C—C, C—OH, C—O—C, and C═O at binding energy of 284.5, 285.3, 286.6 and 287.5 eV, respectively.[39,40] The quantitative composition of PVB surface is calculated to be 61%, 28%, and 11% for vinyl butyral, vinyl alcohol, and vinyl acetate, respectively. The results show that the contents of both vinyl alcohol and vinyl acetate are higher at surface. Therefore, the surface of PVB contains a large amount of the hydrophilic groups which can absorb the water in atmosphere. The water can act as a plasticizer for PVB. Considering the relatively narrow molecular weight distribution and homogeneous chemical composition, the plasticizing effect is not affected by the molecular weight distribution, as similar to other plasticized systems such as plasticized poly(vinyl chloride).

The water content in the films with various thicknesses was measured by the Karl Fischer technique. The samples were kept in an incubator at 25°C under 50% RH for 8 h. It was confirmed that the sample film is in the equilibrium condition regarding the water content after 8 h. As shown in Figure 5, the water content per unit area is proportional to the thickness. Furthermore, the solid line is not started from the origin suggesting that the surface, i.e., zero thickness, contains additional water. The value is found to be 6.90 g/m^2 from the intercept of y-axis. The result qualitatively corresponds with the ATR-FTIR spectra. Moreover, the slope represents the water content inside of the films, which is calculated to be 5.32 wt %. The different in the water content between surface and bulk is attributed to the surface localization of the hydrophilic groups, which also prohibits the diffusion of water to inside of the film.

Figure 6 shows the temperature dependence of dynamic tensile modulus at 10 Hz. The samples were kept in an incubator at 25°C for 8 h; one was under vacuum condition and the other was under 50% RH. The E'' and *tan* δ curves around T_g for the

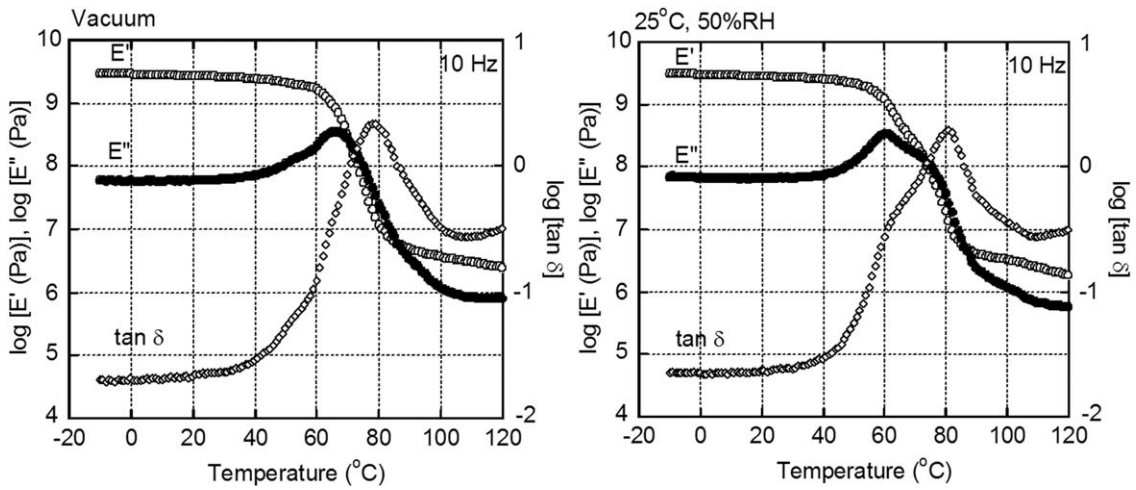

Figure 6. Temperature dependence of (open circles) tensile storage modulus E', (closed circles) loss modulus E'' and (open diamonds) loss tangent tan δ at 10 Hz for the samples kept under (a) vacuum and (b) 25°C and 50% RH.

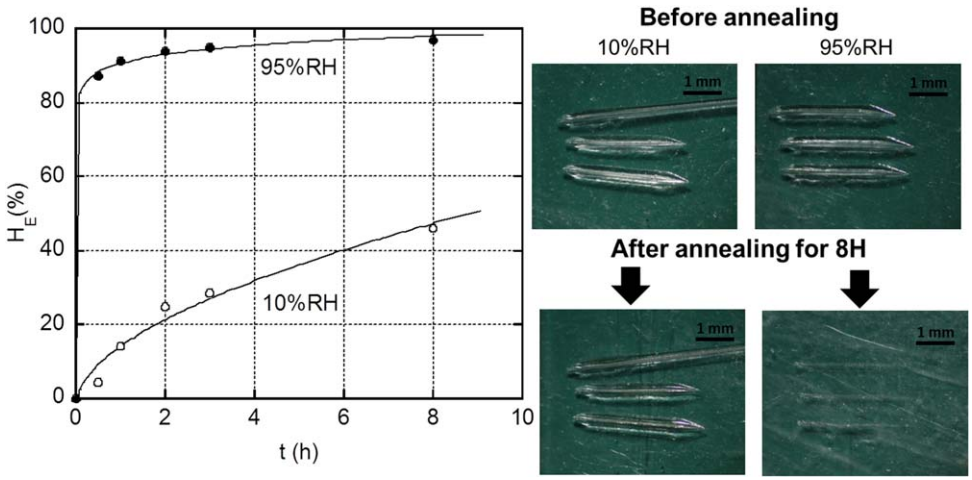

Figure 7. Self-healing behavior at 56°C and 10 or 95% RH; (left) healing efficiency as a function of time and (right) the sample surface at (top) $t = 0$ and (bottom) $t = 8$ h. [Color figure can be viewed in the online issue, which is available at wileyonlinelibrary.com.]

sample kept at 50% RH have ambiguous double peaks; one is located at 80°C and the other is at 60°C. The peak at the higher temperature almost corresponds with that for the sample kept under vacuum. This is attributed to T_g of the bulk. In other words, T_g of the bulk, which contains a small amount of water (5.32 wt %), is not affected by the humidity greatly. In contrast, the peak at the lower temperature is strongly affected by the surface, which is plasticized by a large amount of adsorbed water. The plasticized surface is responsible for the self-healing behavior even at the room temperature.

For the better understanding the effect of humidity, the healing behavior was investigated at different levels of RH, i.e., 10% RH and 95% RH, at 56°C. As shown in Figure 7, the healing of the scar occurs in a short time at the high humidity condition. The healing efficiency is around 90% in an hour. In contrast, the healing occurs slowly at the low humidity. The healing efficiency after 8 h is about 45%. The results demonstrate that the water absorbed on the surface is responsible for the self-healing behavior.

CONCLUSIONS

Good self-healing behavior is detected for PVB even at room temperature without any chemical reaction. Although T_g of PVB is around 76°C, the depth of the applied scar is healed more than 50% at 25°C and 50% RH. The high level of healing efficiency is attributed to the marked molecular motion at surface, which contains a large amount of water owing to the surface localization of vinyl alcohol. The water acts as a plasticizer, and this is confirmed by the dynamic mechanical properties. Consequently, the healing efficiency is greatly enhanced at the high humidity condition because of the marked mobility of polymer chains at surface.

ACKNOWLEDGMENTS

This study was supported by Grand-in-Aid for Scientific Research No. 25410221. I would like to express my appreciation to Associate Professor Dr. Ken Kojio of Kyushu university.

REFERENCES

1. Bergman, S. D.; Wudl, F. *J. Mater. Chem.* **2008**, *18*, 41.
2. Wool, R. P. *Soft. Matter* **2008**, *4*, 400.
3. Wu, D. Y.; Meure, S.; Solomon, D. *Prog. Polym. Sci.* **2008**, *33*, 479.
4. Murphy, E. B.; Wudl, F. *Prog. Polym. Sci.* **2010**, *35*, 223.
5. Zhang, M. Q.; Rong, M. Z. In Handbook of Self-Healing Polymers and Polymer Composites; Zhang, M. Q.; Rong, M. Z., Eds.; John Wiley and Sons, Inc.: Hoboken, **2011**.
6. Binder, W. H. In Handbook of Self-Healing Polymers; Binder, W. H., Eds.; Wiley-VCH: Weinheim, **2013**; Chapter *1*, p 7.
7. White, S. R.; Sottos, N. R.; Geubelle, P. H.; Moore, J. S.; Kessler, M. R.; Sriram, S. R.; Brown, E. N.; Viswanathan, S. *Nature* **2001**, *409*, 794.
8. Jones, A. S.; Rule, J. D.; Moore, J. S.; Sottos, N. R.; White, S. R. *J. R. Soc. Interface* **2007**, *4*, 395.
9. Liu, X.; Sheng, X.; Lee, J. K.; Kessler, M. R.; Kim, J. S. *Compos. Sci. Technol.* **2009**, *69*, 2102.
10. Patel, A. J.; Sottos, N. R.; Wetzel, E. D.; White, S. R. *Compos. Part A* **2010**, *41*, 360.
11. Nesterova, T.; Dam-Johansen, K.; Pedersen, L. T.; Kiil, S. *Prog. Org. Coat.* **2012**, *75*, 309.
12. Dry, C. *Compos. Struct.* **1996**, *35*, 263.
13. Williams, G.; Trask, R.; Bond, I. *Compos. Part A* **2007**, *38*, 1525.
14. Pingkarawat, K.; Wang, C. H.; Varley, R. J.; Mouritz, A. P. *J. Mater. Sci.* **2012**, *47*, 4449.
15. Chujo, Y.; Sada, K.; Saegusa, T. *Macromolecules* **1990**, *23*, 2636.
16. Yoshie, N.; Saito, S.; Oya, N. *Polymer* **2011**, *52*, 6074.
17. Chen, X.; Dam, M. A.; Ono, K.; Mal, A.; Shen, H.; Nutt, S. R.; Sheran, K.; Wudl, F. *Science* **2002**, *295*, 1698.

18. Leibler, L.; Rubinstein, M.; Colby, R. H. *Macromolecules* **1991**, *24*, 4701
19. Beijer, F. H.; Sijbesma, R. P.; Kooijman, H.; Spek, A. L.; Meijer, E. W. *J. Am. Chem. Soc.* **1998**, *120*, 6761.
20. Cordier, P.; Tournilhac, F.; Soulie-Ziakovic, C.; Leibler, L. *Nature* **2008**, *451*, 977.
21. Feldman, K. E.; Kade, M. J.; Meijer, E. W.; Hawker, C. J.; Kramer, E. *J. Macromolecules* **2009**, *42*, 9072.
22. Cui, J.; Campo, A. D. *Chem. Commun.* **2012**, *48*, 9302.
23. Kalista, S. J.; Ward, T. C. *J. R. Soc. Interface* **2007**, *4*, 405.
24. Varley, R. J.; van der Zwaag, S. *Acta. Mater.* **2008**, *56*, 5737.
25. Burattini, S.; Colquhoun, H. M.; Fox, J. D.; Friedmann, D.; Greenland, B. W.; Harris, P. J. F.; Hayes, W.; Mackay, M. E.; Rowan, S. J. *Chem. Commun.* **2009**, *44*, 6717.
26. Hayes, S. A.; Jones, F. R.; Marshiya, K.; Zhang, W. *Compos. Part A* **2007**, *38*, 1116.
27. Hayes, S. A.; Zhang, W.; Branthwaite, M.; Jones, F. R. *J. R. Soc. Interface* **2007**, *4*, 381.
28. Luo, X. F.; Ou, R. Q.; Eberly, D. E.; Singhal, A.; Viratyaporn, W.; Mather, P. T. *ACS. Appl. Mater. Interfaces* **2009**, *1*, 612.
29. Wool, R. P. In Handbook of Polymer Interfaces: Structure and Strength; Wool, R. P., Eds.; Hanser/Gardner: Cincinnati, **1995**; Chapter *2*, p 40.
30. Yamaguchi, M.; Ono, S.; Terano, M. *Mater. Lett.* **2007**, *61*, 1396.
31. Yamaguchi, M.; Ono, S.; Okamoto, K. *Mater. Sci. Eng. B* **2009**, *162*, 189.
32. Yamaguchi, M.; Maeda, R.; Kobayashi, R.; Wada, T.; Ono, S.; Nobukawa, S. *Polym. Int.* **2012**, *61*, 9.
33. Doi, M., Edwards, S. F., Eds. In Handbook of The Theory of Polymer Dynamics; Oxford: UK, **1986**.
34. Brown, H. R.; Yang, A. C. M.; Russell, T. P.; Volksen, W.; Kramer, E. *J. Polymer* **1988**, *29*, 1807.
35. Kajiyama, T.; Tanaka, K.; Takahara, A. *Macromolecules* **1995**, *28*, 3482.
36. Tanaka, K.; Kajiyama, T.; Takahara, A.; Tasaki, S. *Macromolecules* **2002**, *35*, 4702.
37. Tanaka, K.; Ariura, F.; Nagamura, T.; Kajiyama, T. *Polym. J.* **2004**, *36*, 498.
38. Arayachukiat, S.; Siriprumpoonthum, M.; Nobukawa, S.; Yamaguchi, M. *J. Appl. Polym. Sci.* **2014**, *131*, 40337.
39. Pippig, F.; Sarghini, S.; Holländer, A.; Paulussen, S.; Terryn, H. *Surf. Interface. Anal.* **2009**, *41*, 421.
40. Ma, X.; Sun, Q.; Su, Y.; Wang, Y.; Jiang, Z. *Sep. Purif. Technol.* **2007**, *54*, 220.